Eur. Phys. J. Spec. Top.
https://doi.org/10.1140/epjs/s11734-021-00072-6

THE EUROPEAN PHYSICAL JOURNAL SPECIAL TOPICS

Regular Article

Quantum dot and quantum well solar energy converters

Anatoly A. Svidzinsky[1,a] and Marlan O. Scully[1,2,3]

[1] Texas A&M University, College Station, TX 77843, USA
[2] Baylor University, Waco, TX 76798, USA
[3] Princeton University, Princeton, NJ 08544, USA

Received 28 April 2020 / Accepted 5 January 2021

Abstract We review designs of a solar cell constructed from pn junctions, quantum dots and quantum wells. In the first instance we show that quantum wells of varying size embedded in the depletion region yields spatial variation of the energy gap that can be controlled. An advantage of the proposed structure is efficient utilization of the broad solar spectrum, lessening of lattice matching problems and generation of electron-hole pairs in narrow depletion regions which yields fast spatial separation of charges and, thus, reduces recombination losses. In another model we show how quantum coherence can be used, in principle, to eliminate radiative recombination and increase photocell power.

1 Reducing radiative recombination and increasing photocell power

The fundamental limit to photovoltaic efficiency is widely thought to be radiative recombination which balances radiative absorption. However, it is possible to break detailed balance via quantum coherence, which yields, in principle, a quantum limit to photovoltaic operation which can exceed the classical one [1].

The early p-n junction Si solar cells had an efficiency of around 5%. Half a decade later, Shockley and Quiesser [2] showed that the limit was more correctly attributed to the fact that electron-hole pairs are often lost due to radiative recombination. Here we review a toy photocell illuminated by a monochromatic slice of the solar spectrum [1] to show how we can mitigate radiative recombination and enhance efficiency via quantum coherence (see Fig. 1).

In order to explore how quantum coherence could (in principle) be used to mitigate radiative recombination in a solar cell, let us first analyze the quantum dot cell of Fig. 1, in which we inject monochromatic radiation resonant with the energy $\epsilon_c - \epsilon_v$. The populations N_v and N_c are described by the chemical potentials μ_v and μ_c and the ambient temperature T_a so that

$$\frac{N_v}{N_c} = \exp\left(\frac{\epsilon_c - \epsilon_v - (\mu_c - \mu_v)}{k_B T_a}\right) , \tag{1}$$

and the cell voltage is $eV = \mu_c - \mu_v$.

[a] e-mail: asvid@physics.tamu.edu (corresponding author)

The interaction Hamiltonian between the quantum dots and the single mode cavity field is given by

$$\hat{V} = \sum_j \hbar g_j \left|v_j\right\rangle \left\langle c_j\right| \hat{a}^\dagger + \text{adj.} , \tag{2}$$

where g_j is the coupling constant between the jth quantum dot, and the radiation field is described by the creation (annihilation) operators $\hat{a}^\dagger(\hat{a})$. For the present purposes we may model the problem assuming the density matrix for the field, ρ, evolves dynamically as

$$\dot{\rho} = -\int_{t_0}^{t} \frac{dt'}{\hbar^2} \sum_{j,\alpha_j} \left\langle \alpha_j\right| [\hat{V}^j(t,t_0), [\hat{V}^j(t',t_0), \rho(t)\otimes\rho^j]] \left|\alpha_j\right\rangle , \tag{3}$$

where ρ^j is the density matrix for the jth dot. The states of the dot are $|\alpha_j\rangle = |c_j\rangle$ or $|v_j\rangle$ in the notation of Fig. 1b, and t_0 is the time that the jth dot is excited by thermal photon excitation from the n type (donor) or p type (acceptor) reservoir having chemical potential μ_c or μ_v. Upon excitation to the states $|c_j\rangle$ or $|v_j\rangle$ the electrons are modeled as decaying back to the n type or p type reservoir at rate γ. We may include this process by simply taking $\hat{V}^j(t,t_0) \to \hat{V}^j(t,t_0)e^{-\gamma(t-t_0)}$. The summation over dots is replaced by $\sum_j = r\int_{-\infty}^{t} dt_0$, then Eqs. (1)–(3) yield

$$\dot{\rho}(\hat{a},\hat{a}^\dagger,t) = -\kappa\left[\rho_{cc}\left(\hat{a}\hat{a}^\dagger\rho + \rho\hat{a}\hat{a}^\dagger - 2\hat{a}^\dagger\rho\hat{a}\right) + \rho_{vv}\left(\hat{a}^\dagger\hat{a}\rho + \rho\hat{a}^\dagger\hat{a} - 2\hat{a}\rho\hat{a}^\dagger\right)\right] , \tag{4}$$

Published online: 08 April 2021

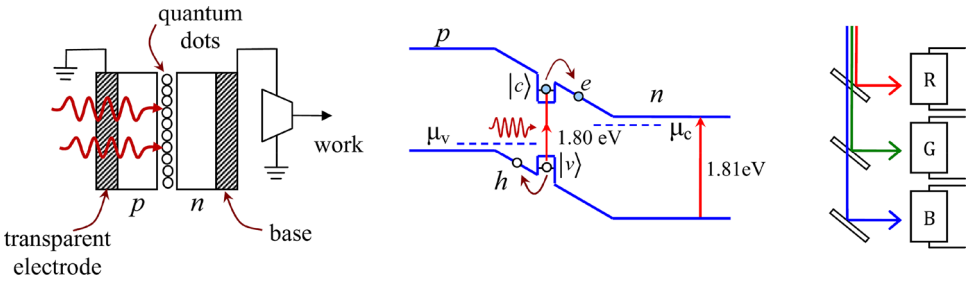

Fig. 1 **a** Schematic of photocell consisting of quantum dots sandwiched between p and n regions. Solar radiation excites electrons from the valence to conduction states in the quantum dots. **b** The "built-in" field in the depletion layer separates electrons and holes; however, they can radiatively recombine before being separated. Absorption in the bulk semiconductor is avoided by ensuring that $\hbar\nu < \epsilon_g$; e.g., in the figure we choose $\hbar\nu = 1.8$ eV and $\epsilon_g = 1.81$ eV. **c** The energy loss by phonon emission from electrons excited well above the band edge can be essentially eliminated by dividing the photon flux into frequency components, each of which is directed to a cell with its band gap matched to the incident light. For example, frequency sensitive beam splitters are here depicted as dividing the solar radiation into red, green, and blue beams which are tuned to the three cells with $\hbar\nu_i < \epsilon_g^i$ where $i = R, G$ and B

where $\rho_{vv}(\rho_{cc})$ is the density matrix probability for finding the valence (conduction) state occupied, r is the rate of scattering of electrons (into and out of the dots) and $\kappa = -rg^2/\gamma^2$.

The equation of motion for the average photon number $\bar{n}$ is given by

$$\begin{aligned}\frac{d\bar{n}}{dt} &= -(R_v - R_c)\bar{n} + R_c \\ &= -R\left[\frac{1}{e^{\hbar\nu/k_BT_S} - 1} - \frac{1}{e^{(\hbar\nu - eV)/k_BT_a} - 1}\right],\end{aligned} \tag{5}$$

where $R_v = \kappa\rho_{vv}$, $R_c = \kappa\rho_{cc}$, $R = R_c - R_v$, and $T_S(T_a)$ is the temperature of the solar radiation (ambient surroundings).

In Eq. (5) we have replaced $\bar{n}$ on the right-hand side by its equilibrium value for solar radiation at temperature T_S. The second term in the square bracket follows from the fact that

$$\frac{R_v}{R_c} = \exp\left(\frac{\hbar\nu - eV}{k_BT_a}\right) \tag{6}$$

since $\rho_{vv}/\rho_{cc} = N_v/N_c$ as it appears in Eq. (1).

As an example of the utility of Eq. (5), we note that at steady state, the second term in the square bracket cancels the first term so that $\hbar\nu/k_BT_S = (\hbar\nu - eV)/k_BT_a$, which yields Carnot efficiency [3]

$$eV = \hbar\nu\left(1 - \frac{T_a}{T_S}\right). \tag{7}$$

Having seen that our toy model contains the essential features of monochromatic photocell operation, we proceed to replace the state $|c\rangle$ by the doublet $|c_1\rangle$, $|c_2\rangle$ which is coupled by a resonant driving field with

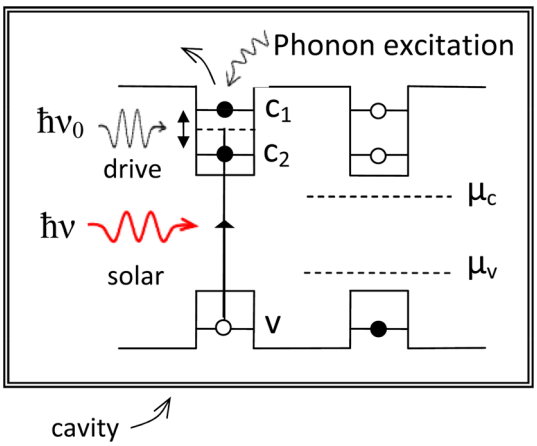

Fig. 2 Quantum dots having upper level conduction band states, $|c_1\rangle$ and $|c_2\rangle$, are coherently driven by a field such that $\hbar\nu_0 = \frac{1}{2}(\epsilon_{c_1} - \epsilon_{c_2})$. The monochromatic solar photons having energy $\hbar\nu$ are tuned to the midpoint between the upper levels. The host semiconductor system, in which the quantum dots are embedded, has effective Fermi energies μ_c and μ_v for the conduction and valence bands

$$\hbar\nu_0 = \frac{1}{2}(\epsilon_{c_1} - \epsilon_{c_2}), \tag{8}$$

as shown in Fig. 2.

We assume that coherent field drives the c_1c_2 transition in resonance with Rabi frequency Ω. Then we transform the driving field away to obtain a new interaction Hamiltonian which treats Ω to all orders and make the secular approximation. The new interaction Hamiltonian reads

$$\hat{V} = \hbar g\,|v\rangle\langle c_2|\,\hat{a}^\dagger + \text{adj.}\,. \tag{9}$$

We then obtain a photon rate equation

$$\frac{d\bar{n}}{dt} = -R\left[\frac{1}{e^{\hbar\nu/k_BT_S}-1} - \frac{1}{e^{(\hbar\nu+\hbar\nu_0-eV)/k_BT_a}-1}\right], \tag{10}$$

which implies

$$eV = \hbar\nu\left(1-\frac{T_a}{T_S}\right)+\hbar\nu_0. \tag{11}$$

That is, we now have a quantum efficiency which exceeds the voltage given by Eq. (7). The preceding coherent drive model illustrates the role of quantum coherence in a simple way. One should mention that it is possible to generate coherence without the use of an external coherent drive. For example, coherence in a photocell can be induced by incoherent solar radiation which can enhance light absorption and increase the cell power [4–6].

Finally we make contact with the quantum Carnot engine [7], which is in some ways similar to the quantum solar cell. In the photo-Carnot heat engine a field is the working fluid. If the field is maintained at thermal equilibrium by hot atoms injected into the cavity, then the engine operates with the usual Carnot efficiency $\eta = 1-T_c/T_h$, where T_h and T_c are the temperatures of the hot energy source and the cold entropy sink. However, if the atoms are injected in a coherent superposition of ground (b) and excited (a) states, the efficiency of this quantum photon engine is given by [7]

$$\eta_Q = \eta - 3\frac{T_c}{T_h}\bar{n}|\rho_{ab}|\cos\varphi, \tag{12}$$

where φ is the phase of the atomic coherence ρ_{ab}. The correspondence with the quantum photocell is clear: In quantum photocell, we use quantum coherence to enhance the transfer of solar energy to the quantum dots. In the quantum photo-Carnot engine, we use quantum coherence to maximize transfer of atomic energy to the photons.

To summarize this section, we ask the question, "Can radiation recombination be avoided?" The answer is yes, in principle. By breaking detailed balance, radiative recombination can be substantially reduced. This can, in principle, enhance the efficiency of photocells, e.g., photodetectors and solar cells; however this is not our key point. It is important to understand the fundamental limits and that radiative recombination can be mitigated.

Next we consider more realistic quantum dot and quantum well solar cells. First we review basic energy conversion processes in photocells and limitations on their efficiency. Then we discuss novel cell designs utilizing broad solar spectrum in Sects. 2.6 and 2.7.

2 Quantum dot and quantum well solar convertors

An efficient cell must be able to convert most of solar photons (with broad energy spectrum from 0.5 to 3.5 eV) into electric energy. Due to thermalization losses and lack of absorption of photons with energy less than band gap a single pn junction-type solar cell is not very efficient [3]. Efficiency can be increased in tandem cells by offering the solar cell only photons within the narrow energy interval and processing the other photons by cells with a different band gap [8]. The upper limit for the efficiency of an infinite tandem is 86% for concentrated radiation [3]. However, high-efficiency multiple-junction solar cells can be fabricated only from a limited set of materials that can provide lattice matching. The most presently efficient (about $44-47\%$) solar cells are multijunction devices [9–13]. Efficiency can be increased by reducing absorption and thermalization losses provided that other possible limitations, e.g. internal resistance, remain small.

Introduction of quantum wells, dots or nanocryastals into solar cell physics is interesting and promising [14–16]. Matching the electronic excitation energy (band gap) to the solar spectrum is a central problem in semiconductor solar cells, see Fig. 3. Photovoltaic cells with array of quantum wells or dots have been studied in various publications. In particular, cell fabrication [17], materials [18], performance [19,20] and charge transport [21] are the subjects of recent investigation.

Here we propose a design of a tandem solar energy convertor made of the same wide band gap semiconductor with quantum wells (or dots) embedded in the depletion region. Variation of the well (dot) size yields spatial variation of the energy gap in the depletion region. This differs from conventional tandem cells in which energy gap is uniform in each pn junction. A decrease in the energy gap in the depletion region away from the photosensitive surface provides effective absorption of photons in a certain energy range by each element of the cascade resulting in a higher utilization efficiency of solar radiation. In the proposed scheme, electrons (holes) move through the depletion region by quantum tunneling from one well (dot) to another.

Advantage of the proposed design is lessening of the lattice matching problem since only two different materials (the bulk semiconductor and material for quantum wells) are needed. In addition, in the present design, generation of electron-hole pairs occurs in narrow depletion regions which yields fast spatial separation of charges and, thus, reduces recombination losses.

To put the present work in perspective we next review limitations on the pn junction solar cell efficiency in details.

2.1 Individual energy conversion processes in solar cells

There are various contributions to the solar cell losses. Some of them have been made small in the most effi-

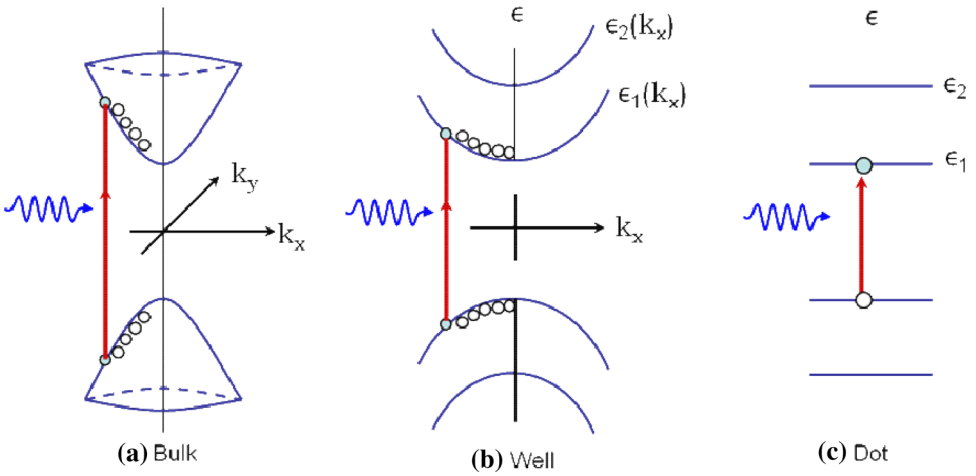

Fig. 3 **a** Electronic states in a bulk (3D) semiconductor with gap $E_g = E_c - E_v$. A photon with energy $E > E_g$ promotes electrons from the valence to the conduction band. Electrons move to the bottom of the conduction band via phonon emission. Likewise holes raise to the top of the valence band emitting phonons. **b** Electrons and holes on a 2D quantum well have a discrete energies together with free particle energy bands in directions parallel to the walls of the well, which also involve phonon emission. **c** In a 1D quantum dot only discrete energy are allowed and multiple phonon emission is not involved

cient cells, e.g., surface reflection, internal resistance, absorption in the inactive window layers, contact voltage, nonradiative recombination, etc. However, other processes substantially limit the cell efficiency. Those are shown in Figs. 4 and 5 and subject of the present discussion. The overall efficiency η of the solar cell is given by the product of the efficiencies of the individual energy conversion processes [3]

$$\eta = \eta_{\text{absorption}} \cdot \eta_{\text{thermalization}} \cdot \eta_{\text{thermodynamic}} \cdot FF \quad (13)$$

where the absorption efficiency $\eta_{\text{absorption}}$ is the fraction of photons absorbed by the solar cell. It accounts for the photons with energy smaller than the gap which are not absorbed. $\eta_{\text{thermalization}}$ accounts for losses due to thermalization of the electron-hole pairs with energy greater than the gap which loose the excess energy emitting phonons. Thermodynamic efficiency $\eta_{\text{thermodynamic}}$ and Fill Factor FF appear due to finite temperature of the cell T.

2.2 Thermodynamic limit on solar cell efficiency

Laws of thermodynamics impose an upper limit on voltage at which solar cell can operate constraining the cell efficiency ($\eta_{\text{thermodynamic}}$ in Eq. (13)). The voltage is maximum for open circuit. Next we estimate the maximum value of the open circuit voltage V_{oc}. When an electron undergoes transition from the conduction band to the valence band, the Helmholtz free energy released is equal to eV

$$eV = E_g - T\Delta S, \quad (14)$$

where V is the voltage across the pn junction, E_g and ΔS are the internal energy and entropy lost by the semiconductor. To find ΔS one can assume that under open circuit condition the electron goes from the conduction band to the valence band by recombination with a hole and emitting a photon. Then ΔS is equal to increase in the entropy of the photon gas

$$S = k_B \sum_{\mathbf{k}} \left[(n_{\mathbf{k}} + 1) \ln(n_{\mathbf{k}} + 1) - n_{\mathbf{k}} \ln(n_{\mathbf{k}}) \right], \quad (15)$$

where summation is over all possible photon modes $\mathbf{k}$ and $n_{\mathbf{k}}$ is the number of photons in mode $\mathbf{k}$. When an additional photon of energy E_g is added to the mode $\mathbf{k}$ the change in entropy is

$$\Delta S = k_B \ln\left(1 + \frac{1}{n_{\mathbf{k}}}\right). \quad (16)$$

Substituting Eq. (16) into Eq. (14) we obtain

$$eV = E_g - k_B T \ln\left(1 + \frac{1}{n_{\mathbf{k}}}\right), \quad (17)$$

or

$$n_{\mathbf{k}} = \frac{1}{\exp[(E_g - eV)/k_B T] - 1}, \quad (18)$$

where T is the semiconductor temperature.

Let us assume that we decompose the incident light into narrow spectral intervals and treat each spectral component separately. For monochromatic light with frequency ω one can choose material with band gap $E_g = \hbar\omega$ to avoid absorption and thermalization losses. The radiative current (due to electron-hole recombination) and current due to absorbed solar light are

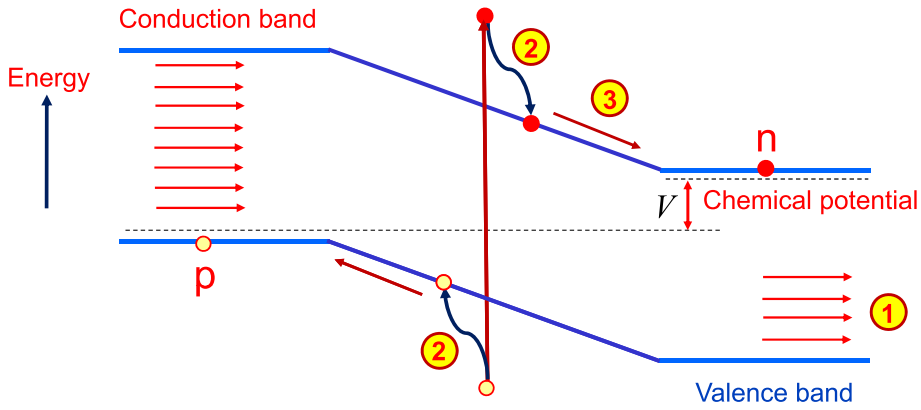

Fig. 4 Main contributions to solar cell losses: (1) Photons with energy less then gap are not absorbed (absorption losses); (2) Electrons (holes) with excess energy are quickly relaxing to the bottom (top) of the conduction (valence) band by phonon emission (thermalization losses); (3) Losses due to finite temperature of the cell (thermodynamic losses and Fill Factor)

$$J_{\rm rad} \propto \sum_{\mathbf{k}} n_{\mathbf{k}} \propto \frac{\Omega_{\rm emit}}{\exp[(E_g - eV)/k_BT] - 1}, \quad (19)$$

$$J_{\rm Sun} \propto \frac{\Omega_{\rm Sun}}{\exp[E_g/k_BT_S] - 1}, \quad (20)$$

where $\Omega_{\rm emit}$ and $\Omega_{\rm Sun}$ are the solid angle of the emitted radiation and the solid angle of the Sun viewed from the cell, T_S is the temperature of the solar surface. The factors $\Omega_{\rm emit}$ and $\Omega_{\rm Sun}$ appear due to summation over degenerate photons modes $\mathbf{k}$ with energy E_g. For open circuit $J_{\rm rad} = J_{\rm Sun}$ which yields the following expression for the open circuit voltage

$$eV_{\rm oc} = E_g - k_BT \ln\left[1 + \frac{\Omega_{\rm emit}}{\Omega_{\rm Sun}}\left(\exp\left(\frac{E_g}{k_BT_S}\right) - 1\right)\right]. \quad (21)$$

Thus the thermodynamic efficiency for the narrow spectral interval is

$$\eta_{\rm thermodynamic} = \frac{eV_{\rm oc}}{E_g} = 1 - \frac{k_BT}{E_g} \ln\left[1 + \frac{\Omega_{\rm emit}}{\Omega_{\rm Sun}}\left(\exp\left(\frac{E_g}{k_BT_S}\right) - 1\right)\right]. \quad (22)$$

Without light focusing $\Omega_{\rm Sun} = 6.8\times10^{-5}$. If $\Omega_{\rm emit} = 4\pi$, $E_g = 1.35$ eV, $k_BT_s = 0.5$ eV and $k_BT = 0.0259$ eV we find $V_{\rm oc} = 0.97$ Volts and

$$\eta_{\rm thermodynamic} = 0.72. \quad (23)$$

Focusing solar radiation increases $\Omega_{\rm Sun}$. This is the case because during passage through a nonabsorbing and nonemitting ideal imaging system, the energy current density per solid angle remains unchanged. Thus, if light intensity increases the solid angle also increases. Maximum efficiency is achieved for $\Omega_{\rm Sun} = \Omega_{\rm emit}$ and

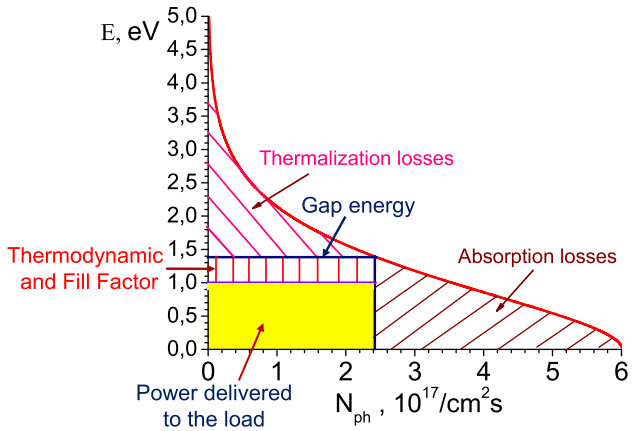

Fig. 5 Graphical representation of single junction solar cell losses. Solid curve shows number of solar photons N_{ph} per unit area and unit time with energy greater then E as a function of E. Area under the curve is equal to the total solar power density. Various contributions to the cell losses are shown as hatched areas

Eq. (22) yields the Carnot efficiency

$$\eta_{\rm thermodynamic} = 1 - \frac{T}{T_S} \quad (24)$$

which is independent of the photon energy.

2.3 Fill Factor FF

One of the limitations on the solar cell efficiency is the Fill Factor which determines what fraction of the stored chemical energy the solar cell can deliver operating at the maximum power point

$$FF = \frac{j_{\rm mp}V_{\rm mp}}{j_{\rm sc}V_{\rm oc}}, \quad (25)$$

where $j_{\rm mp}$ and $V_{\rm mp}$ are the current and voltage at the maximum power point, $j_{\rm sc}$ is the short-circuit current and $V_{\rm oc}$ is the open-circuit voltage.

For pn junction the current-voltage characteristic reads

$$j = j_S \left[\exp\left(\frac{eV}{k_BT}\right) - 1\right] + j_{\rm sc}, \tag{26}$$

where j_S is the reverse saturation current. Eq. (26) gives the following relation between $j_{\rm sc}$ and $V_{\rm oc}$

$$\frac{j_{\rm sc}}{j_S} = 1 - \exp\left(\frac{eV_{\rm oc}}{k_BT}\right). \tag{27}$$

The condition of maximum power yields

$$d(jV) = 0, \tag{28}$$

or

$$\frac{dj}{dV} = -\frac{j}{V}. \tag{29}$$

Taking into account Eq. (26) we find

$$\frac{ej_S}{k_BT}\exp\left(\frac{eV_{\rm mp}}{k_BT}\right) = -\frac{j_{\rm mp}}{V_{\rm mp}}, \tag{30}$$

which using Eqs. (27) and (26) yields

$$V_{\rm mp} = \frac{k_BT}{e}\left[\exp\left(\frac{e(V_{\rm oc} - V_{\rm mp})}{k_BT}\right) - 1\right], \tag{31}$$

or

$$V_{\rm mp} = V_{\rm oc} - \frac{k_BT}{e}\ln\left[1 + \frac{eV_{\rm mp}}{k_BT}\right]. \tag{32}$$

Approximately one can replace $V_{\rm mp}$ by $V_{\rm oc}$ under the logarithm and obtain

$$V_{\rm mp} \approx V_{\rm oc} - \frac{k_BT}{e}\ln\left[1 + \frac{eV_{\rm oc}}{k_BT}\right]. \tag{33}$$

One can see that $V_{\rm mp}$ depends only on $V_{\rm oc}$ and temperature T.

Eqs. (25), (26), (27) and (33) yield

$$FF = \frac{x - \ln(1+x)}{1+x}, \quad \text{where} \quad x = \frac{eV_{\rm oc}}{k_BT}. \tag{34}$$

That is Fill Factor also depends only on $V_{\rm oc}$ and T. For $V_{\rm oc} = 0.97$ Volt and $T = 300$ K we find $x = 39$ and $FF = 0.88$.

Using Eq. (22) we obtain

$$\eta_{\rm thermodynamic} \cdot FF = 0.63 \tag{35}$$

which gives an upper limit on efficiency of a monochcomatic light cell without radiation focusing.

For fully focused solar light $eV_{\rm oc} = E_g(1 - T/T_S) = 1.35 \cdot 0.95 = 1.28$ eV. Thus $FF = 0.90$ and

$$\eta_{\rm thermodynamic} \cdot FF = 0.86 \tag{36}$$

which is maximum efficiency of a cell for concentrated monochcomatic radiation.

2.4 Absorption efficiency and thermalization losses

If electron-hole pairs are created with the energy E greater than band gap E_g the excess energy $E - E_g$ is lost due to fast electron-phonon collisions (thermalization losses). Assuming black-body solar spectrum this yields

$$\eta_{\rm thermalization} = \frac{E_g \int_{E_g}^{\infty} dE \frac{E^2}{\exp(E/k_BT_S)-1}}{\int_{E_g}^{\infty} dE \frac{E^3}{\exp(E/k_BT_S)-1}}. \tag{37}$$

In addition, solar photons with energy $E < E_g$ are not absorbed, thus

$$\eta_{\rm absorption} = \frac{\int_{E_g}^{\infty} dE \frac{E^3}{\exp(E/k_BT_S)-1}}{\int_{0}^{\infty} dE \frac{E^3}{\exp(E/k_BT_S)-1}} \tag{38}$$

and, therefore,

$$\eta_{\rm absorption} \cdot \eta_{\rm thermalization} = \frac{E_g}{k_BT_S} \frac{\int_{E_g/k_BT_S}^{\infty} dx \frac{x^2}{\exp(x)-1}}{\int_{0}^{\infty} dx \frac{x^3}{\exp(x)-1}}. \tag{39}$$

The right hand side of Eq. (39) is maximum for $E_g = 2.17k_BT_S = 1.09$ eV which gives the maximum absorption-thermalization efficiency for a single pn junction cell

$$\eta_{\rm absorption} \cdot \eta_{\rm thermalization} = 0.44. \tag{40}$$

Thus, a single pn junction solar cell cannot have efficiency exceeding 44% even if cell operates at zero temperature. Taking into account $\eta_{\rm thermodynamic}$ and Fill Factor for $T = 300$ K reduces the net limiting efficiency to (cf. Ref. [2])

$$\eta = 0.265 \tag{41}$$

for unconcentrated solar radiation (optimum gap is $E_g = 2.76k_BT_S = 1.38$ eV) and to

$$\eta = 0.37 \tag{42}$$

for full concentration (optimum gap is $E_g = 2.30k_BT_S = 1.15$ eV).

It is worth to note that efficiency experimentally achieved for a champion single pn junction cell (GaAs cell with $E_g = 1.41$ eV) and AM1.5 solar spectrum is $\eta = 0.253$ [22] which is very close to the answer given by Eq. (41). Such agreement indicates that losses not included into the present discussion give much smaller contribution.

One can improve the absorption efficiency and reduce thermalization losses in tandem cells by offering each pn junction only photons within the narrow energy interval and processing the other photons by materials with a different band gap [8]. Tandem cells made of semiconductors with different band gaps are used in satellites where high cell efficiency is required.

2.5 Triple-junction tandem solar cell

Monolithic multijunction solar cells have produced the highest efficiencies practically achievable. In particular, Sharp Corporation is claiming an efficiency record of a triple-junction compound semiconductor device that boasts a 37.9% efficiency for unconcentrated light and 44.4% efficiency using concentrator systems [23]. Six-junction solar cells demonstrated 47.1% conversion efficiency under 143 Suns concentration and 39.2% for unconcentrated light [13].

Next we discuss maximum efficiency of a solar cell made of three pn junctions (with energy gaps $E_{g1} > E_{g2} > E_{g3}$) connected in series. The top junction absorbs photons with energy $E > E_{g1}$, while the other two junctions utilize photons with $E_{g2} < E < E_{g1}$ and $E_{g3} < E < E_{g2}$ respectively. To match current through the junctions we must impose a constraint that each junction absorbs the same number of photons, which gives two equations on the three unknown values E_{g1}, E_{g2} and E_{g3}

$$\int_{E_{g3}}^{E_{g2}} dE \frac{E^2}{\exp\left(\frac{E}{k_B T_S}\right) - 1} = \int_{E_{g2}}^{E_{g1}} dE \frac{E^2}{\exp\left(\frac{E}{k_B T_S}\right) - 1} = \int_{E_{g1}}^{\infty} dE \frac{E^2}{\exp\left(\frac{E}{k_B T_S}\right) - 1}. \tag{43}$$

Maximization of the $\eta_{\text{absorption}} \cdot \eta_{\text{thermalization}}$ efficiency yields the third constraint

$$\eta_{\text{absorption}} \cdot \eta_{\text{thermalization}} = \frac{(E_{g1} + E_{g2} + E_{g3})}{E_a} \frac{\int_{E_{g1}}^{\infty} dE \frac{E^2}{\exp(E/k_B T_S) - 1}}{\int_0^{\infty} dE \frac{E^2}{\exp(E/k_B T_S) - 1}} = \max, \tag{44}$$

where $E_a = 1.35$ eV is the average energy of solar photons. Eqs. (43) and (44) give the following optimum parameters

$$E_{g1} = 1.77 \text{ eV}, \quad E_{g2} = 1.12 \text{ eV}, \quad E_{g3} = 0.61 \text{ eV}, \quad \eta_{\text{absorption}} \cdot \eta_{\text{thermalization}} = 0.69. \tag{45}$$

To account for the thermodynamic efficiency and Fill Factor we must multiply each E_{gi} by $\eta_{\text{thermodynamic}} \cdot FF$ which gives an extra factor

$$\frac{eV}{E_{g1} + E_{g2} + E_{g3}} = \frac{\sum_{i=1}^{3} E_{gi} \cdot \eta_{\text{thermodynamic}} \cdot FF}{E_{g1} + E_{g2} + E_{g3}}. \tag{46}$$

Here $\eta_{\text{thermodynamic}} \cdot FF$ depend on E_{gi} and given by

$$\eta_{\text{thermodynamic}} \cdot FF = \left(1 - \frac{k_B T}{E_{gi}} \ln\left[1 + \frac{\Omega_{\text{emit}}}{\Omega_{\text{Sun}}}\left(\exp\left(\frac{E_{gi}}{k_B T_S}\right) - 1\right)\right]\right) \cdot \left(\frac{x_i - \ln(1 + x_i)}{1 + x_i}\right), \tag{47}$$

where

$$x_i = \frac{E_{gi}}{k_B T} - \ln\left[1 + \frac{\Omega_{\text{emit}}}{\Omega_{\text{Sun}}}\left(\exp\left(\frac{E_{gi}}{k_B T_S}\right) - 1\right)\right]. \tag{48}$$

This yields for unconcentrated light the net efficiency

$$\eta = 0.41. \tag{49}$$

For full concentration we obtain

$$\eta = 0.58, \tag{50}$$

while for partial focusing, $\Omega_{\text{Sun}} = 500 \times 6.8 \times 10^{-5}$, we find

$$\eta = 0.51. \tag{51}$$

It is interesting to note that the record efficiency achieved for the triple-junction solar cell for unconcentrated light is only a few percent less than the limiting value given by Eq. (49). Such a cell is made of InGaP (top layer), GaAs (middle layer) and InGaAs (bottom layer) [23]. The corresponding energy gaps are 1.87 eV, 1.4 eV and 1.0 eV respectively [24]. However, according to Eq. (45), combination of band-gaps for this triple-junction structure is not optimal. One can optimize band-gaps of the triple-junction cell by reducing band-gaps of top and middle cells. So, band-gap combination of 1.7 eV (AlGaAs), 1.2 eV (InGaAs) and 0.65 eV is the optimal structure including Ge bottom cell [24].

In principle, by increasing the number of pn junctions with different gaps in the tandem one can further reduce absorption and thermalization losses. However, use of different materials yields the lattice matching problem.

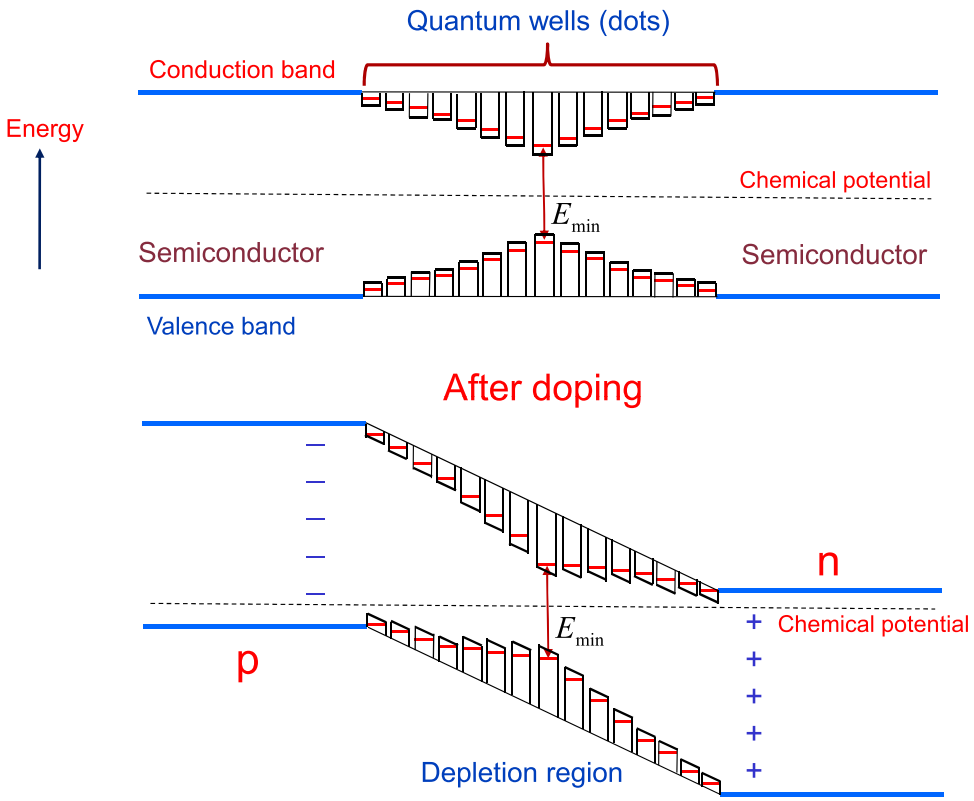

Fig. 6 Proposed structure of a solar cell element with quantum wells (dots) embedded in the depletion region of pn junction. Energy gap first gradually decreases and then increases upto its initial value inside the depletion region

If lattice constants are not matched the internal stress develops at the interfaces resulting in appearance of cracks and defects which, in turn, increase the cell internal resistance. The increased resistance becomes a limiting factor of multi junction devices constraining further improvement of the cell performance.

Next we discuss a possible design of tandem cells with quantum wells (dots) in the depletion region which lessens the lattice matching problem by using only two different materials (the bulk semiconductor and material for quantum wells).

2.6 Cell design utilizing broad solar spectrum

The proposed structure of the solar cell element is shown in Fig. 6. The element is made of a wide band gap semiconductor (e.g., GaN, with $E_g = 3.4$ eV) so that practically no solar photons have energy larger than the gap. The depletion region of the pn junction is filled with quantum wells (dots). The well (dot) size gradually changes across the junction yielding energy levels shown in Fig. 6. Each quantum well (dot) is made of the same material in which energy of the conduction and valence bands is controlled by varying the well size. Value of the chemical potential in each well can be controlled independently by doping.

Solar energy convertor is a tandem of several (about 10) pn junctions made of the same semiconductor and connected in series (see Fig. 7). Each cell element utilizes a certain portion of the solar spectrum. Light first enters the p-layer as sketched in the Fig. 7. High energy photons are absorbed in the first pn depletion region and produce electron-hole pairs in quantum wells (dots). Namely, all photons with energy $E > E_{g1}$ are absorbed, where E_{g1} is determined by the smallest value of the gap in the depletion region. Electrons (holes) move through the depletion region by quantum tunneling from one well (dot) to another. In Appendix A we show that in order to have necessary tunneling rate the spacing between wells (dots) should be less than about 1 nm. Energy levels in adjacent wells (dots) are separated by some amount so that electrons flow from higher to lower energy level. The energy separation should be smaller than the Debye energy E_D which is typically a few 0.01 eV. In such a case the excess energy goes into emission of acoustic phonons which is an efficient mechanism of energy sink. At zero temperature the voltage across the first pn junction would be about $eV_1 = E_{g1}$. Electron-hole pairs generated with energy larger than E_{g1} loose the excess energy during propagation through the depletion region by emitting phonons. Electrons and holes flow in the opposite directions and become spatially separated (electrons are accumulated in the conducting band of n-region and holes are in the valence band of p-region).

Electrons flowing out of the n-layer of the left pn junction and holes flowing out of the p-layer of the right pn junction recombine in a tunnel junction as shown in Fig. 7. Usually tunnel junction is made of a heavily doped semiconductor [25]. Tunnel barrier allows us to avoid a negative voltage at the np interface which would reduce the cell efficiency. In the tunnel junction, elec-

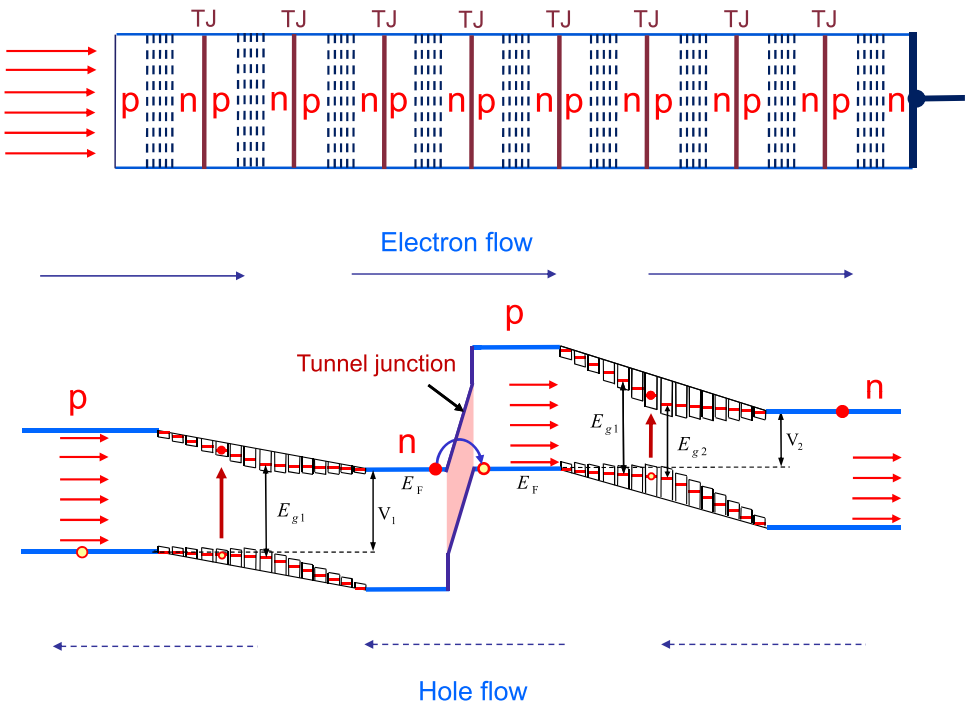

Fig. 7 Structure of solar energy convertor with series pn junction layers containing quantum wells (dots) in the depletion regions. n and p-type layers are connected by a tunnel junction

trons and holes belong to the same Fermi distribution and recombination proceeds without a difference in the chemical potentials.

In the second pn junction the minimum gap of quantum wells is $E_{g2} < E_{g1}$ and all photons with energy $E_{g2} < E < E_{g1}$ are absorbed in that region. Voltage across the second junction is about $eV_2 = E_{g2}$. And so on, until the whole solar spectrum is covered. Because junctions are connected in series the electric current through each junction is the same. As a result, energy intervals $[E_{g,n+1}, E_{gn}]$ must be chosen such that the numbers of solar photons in each interval are equal. For a black-body spectrum with temperature $k_B T_S = 0.5$ eV the number of photons in the interval $[E_{g,n+1}, E_{gn}]$ is proportional to

$$\Delta N \propto \int_{E_{g,n+1}}^{E_{gn}} dE \frac{E^2}{\exp\left(\frac{E}{k_B T_S}\right) - 1}. \tag{52}$$

As an example we next discuss 9-junction solar cell.

2.7 9-junction solar cell

If each pn junction captures 10% of the solar photons then spectral energy range captured by the junctions should be (in eV): $[2.5, \infty]$, $[2, 2.5]$, $[1.66, 2]$, $[1.4, 1.66]$, $[1.18, 1.4]$, $[0.98, 1.18]$, $[0.79, 0.98]$, $[0.6, 0.79]$, $[0.39, 0.6]$. That is the smallest value of the quantum wells (dots) gap in the junction depletion region should be 2.5, 2, 1.66, 1.4, 1.18, 0.98, 0.79, 0.6, and 0.39 eV respectively. If the cell temperature is zero the net voltage across the cell will be (in eV)

$$\begin{aligned} eV &= E_{g1} + E_{g2} + \ldots + E_{g9} \\ &= 2.5 + 2 + 1.66 + 1.4 + 1.18 + 0.98 + 0.79 \\ &\quad +0.6 + 0.39 = 11.5 \text{ eV}. \end{aligned} \tag{53}$$

The average energy of solar photons is $E_a = 1.35$ eV. Thus efficiency of a solar cell containing 9 pn junctions cannot be larger than

$$\eta = \frac{0.1 \cdot 11.5}{1.35} = 0.85. \tag{54}$$

Eq. (54) describes only contribution to the efficiency due to absorption and thermalization losses. To account for the finite cell temperature T (thermodynamic efficiency and Fill Factor) we must multiply each E_{gi} in Eq. (53) by $\eta_{\text{thermodynamic}} \cdot FF$ given by Eq. (47). We assume that at maximum power the current through each pn junction is equal to j_{sc}, which is a good approximation. Thus the maximum power current is approximately the same for all junctions. For unconcentrated light we take $\Omega_{\text{Sun}} = 6.8 \times 10^{-5}$, $\Omega_{\text{emit}} = 4\pi$, $k_B T_s = 0.5$ eV, $k_B T = 0.0259$ eV and obtain

$$\begin{aligned} eV &= 2.5 \cdot 0.77 + 2 \cdot 0.73 + 1.66 \cdot 0.68 \\ &\quad +1.4 \cdot 0.64 + 1.18 \cdot 0.59 + \\ &\quad 0.98 \cdot 0.52 + 0.79 \cdot 0.44 + 0.6 \cdot 0.3 \\ &\quad +0.39 \cdot 0.07 = 7.17 \text{ eV}, \end{aligned} \tag{55}$$

so that the net efficiency of a solar cell containing 9 pn junctions without light concentration is

$$\eta = 0.53. \tag{56}$$

For full concentration $\Omega_{\rm emit} = \Omega_{\rm Sun}$ and we obtain

$$\begin{aligned} eV = & 2.5 \cdot 0.89 + 2 \cdot 0.88 + 1.66 \cdot 0.87 \\ & + 1.4 \cdot 0.86 + 1.18 \cdot 0.85 + \\ & 0.98 \cdot 0.83 + 0.79 \cdot 0.81 \\ & + 0.6 \cdot 0.78 + 0.39 \cdot 0.72 = 9.84 \text{ eV}, \end{aligned} \quad (57)$$

so that the net efficiency is

$$\eta = 0.73. \quad (58)$$

For partial focusing, e.g. 500 Suns, we find

$$\eta = 0.63. \quad (59)$$

2.8 Infinite tandem

In an ideal case of infinite number of pn junctions there are no absorption and thermalization losses and the net efficiency is given by

$$\eta = \frac{\int_0^\infty dE \frac{E^3}{\exp(E/k_B T_S)-1} \cdot \eta_{\rm thermodynamic} \cdot FF}{\int_0^\infty dE \frac{E^3}{\exp(E/k_B T_S)-1}}, \quad (60)$$

where $\eta_{\rm thermodynamic} \cdot FF$ as a function of E is given by Eq. (47). Integration of Eq. (60) yields for unconcentrated light

$$\eta = 0.65. \quad (61)$$

For full concentration we obtain

$$\eta = 0.86, \quad (62)$$

while for $500 \times 6.8 \times 10^{-5}$ Suns

$$\eta = 0.76. \quad (63)$$

3 Discussion

We here present a (potentially) realizable design which can yield efficiencies better than 80% for focused solar radiation. The present scheme involves making quantum well or quantum dot structures with specific energy levels. In the case of a semiconductor quantum dot, the effective gap is given in the conventional notation by

$$E_g \cong E_g^{\rm bulk} + \frac{k^2\pi^2}{8r^2}\left(\frac{1}{m_e^*} + \frac{1}{m_h^*}\right) \quad (64)$$

where $m_e^*(m_h^*)$ is the effective mass of the electron (hole), r is the dot radius and k is an integer. Thus effective gap can be controlled by changing size of the quantum dot (or size of the quantum well). Accurate selection of quantum dots with specific gap values is crucial for the proposed design. We discus a possible way of quantum dot processing with high precision in Appendix B.

Several points concerning the photovoltaics should be noted. For example, photon absorption only takes place in the quantum wells (dots). Those are located in the depletion region where the pn junction "built in" electric field acts to drive holes into the p doped and electrons into the n doped regions. Furthermore, the electron-hole pairs will be swept from the junction in a time short compared to the recombination time so there will be no recombination of electrons and holes in the depletion layer. Absorption in the bulk n and p type materials to the left and right of the depletion region is undesirable as the electrons and hole excitons will tend to recombine before they can be separated. Such absorption is avoided by tailoring the p and n regions to have a wide energy gap.

Proceeding to analyze the absorption of a beam of intensity I_0 as it passes through the layer of quantum dots of thickness z we write [26]

$$I = I_0 e^{-z/l_{\rm abs}}, \quad (65)$$

where the absorption length $l_{\rm abs}$ is given by

$$\frac{1}{l_{\rm abs}} \cong \frac{3m}{8\pi} N\lambda^2 \frac{\Delta\nu_{\rm rad}}{\Delta\nu_{\rm tot}}, \quad (66)$$

$m\,(\simeq 4)$ is the number of excitons per dot, N is the dot concentration (dots/cm^3), λ is the radiation wavelength, while $\Delta\nu_{\rm rad}$ and $\Delta\nu_{\rm tot}$ are the radiative and total linewidths. We may estimate $l_{\rm abs}$ by considering a uniform layer filled with 5 nm dots, having a concentration $N \cong 10^{18}{\rm cm}^{-3}$. Other parameters are $\lambda = 1\mu$m, $\Delta\nu_{\rm rad} \simeq 10^7\,{\rm s}^{-1}$. The total linewidth is primarily governed by phase diffusion. At the room temperature, as is shown in [27,28] $\Delta\nu_{\rm tot} \cong 10^{12}\,{\rm s}^{-1} = 0.004$ eV. Using the preceding estimates this yields $l_{\rm abs} \approx 0.2\ \mu$m.

Thus, the depletion region of $L = 1\ \mu$m width filled with quantum dots can absorb spectrum in the energy range $\Delta E \sim \Delta\nu_{\rm tot} L/l_{\rm abs} = 0.02$ eV. Therefore, in order to cover the 3 eV wide solar spectrum we need to make about 150 pn junctions with quantum dots. In the case of quantum wells the number of junctions can be much smaller. The point is that each quantum well can absorb radiation with the energy above the well's gap and, thus, the energy range is not limited by the linewidth. Above the gap, radiation is absorbed within the length $l_{\rm abs}$ which is typically of the order of or smaller than the size of the depletion region. Hence, the whole solar spectrum can be covered with only a few pn junctions with quantum wells embedded in the depletion regions. Due to better absorption efficiency of light by quantum wells their use in the proposed design is more promising.

In Appendix D we discuss absorption of light by quantum wells and estimate absorption length $l_{\rm abs}$. It

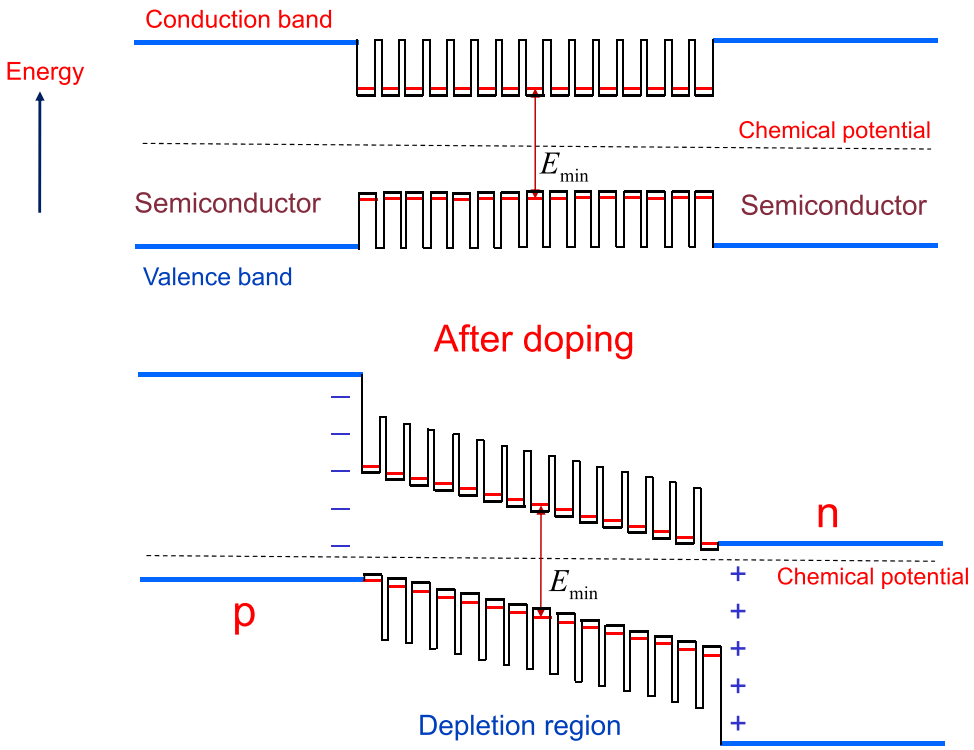

Fig. 8 Proposed structure of a solar cell element with quantum wells embedded in the depletion region of pn junction. Energy gap is constant inside the depletion region which yields efficient absorption of solar photins with $E > E_{min}$ by each part of the depletion region

turns out that l_{abs} for bulk materials can be used as a good estimate of absorption in quantum well structures. The necessary number of QWs can be then obtained simply by dividing the bulk absorption length by the QW thickness. Most materials (e.g., GaAs or InP) have absorption length of the order of 1 μm in the vicinity of the band gap (that is in the energy range useful for photovoltaic). Thus, for 5 nm thick wells in order to have efficient absorption one should put about 200 QWs in each pn junction. Such stack of wells matches the absorption length. Only materials with wide bang gap (such as GaN) have substantially shorter absorption length (about 0.1 μm).

To improve absorption efficiency by quantum wells one can design cell elements to have a constant energy gap E_g in the depletion region as shown in Fig. 8. In such a design, all photons with energy $E > E_g$ are absorbed by each part of the depletion region which reduces the number of quantum wells necessary to absorb solar radiation. Also, if quantum wells (dots) are the same, then such an element is easier to manufacture. However, for such a design the tunneling barrier between quantum wells is higher than for the varying gap design of Fig. 6.

Acknowledgements This work was supported by the Air Force Office of Scientific Research (Grant No. FA9550-20-1-0366 DEF), the Office of Naval Research (Awards N00014-20-1-2184 and N00014-16-1-2578), the Robert A. Welch Foundation (Award A-1261), and National Science Foundation (Grant No. PHY-2013771)

Appendix A Flow of electrons through depletion region

Electrons (holes) generated in quantum wells (dots) by photon absorption can propagate through the depletion region by quantum tunneling mechanism. Namely, electrons (holes) flow from one quantum well (dot) to another by tunneling through the potential barrier in the region between adjacent wells or dots (see Fig. 9). Next we estimate spacing between wells (dots) for which tunneling is efficient.

To estimate electron tunneling rate we approximate spacing between wells (dots) as one dimensional potential barrier

$$V(x) = \begin{cases} U, & 0 < x < a \\ 0, & \text{otherwise} \end{cases} . \qquad \text{(A1)}$$

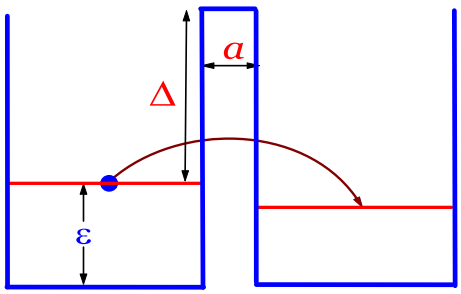

Fig. 9 Electron tunneling between quantum wells

Tunneling probability for electron is given by

$$D = \frac{1}{1 + \frac{U^2}{4\varepsilon\Delta}\sinh^2\left(\frac{\sqrt{2m\Delta}a}{\hbar}\right)}, \tag{A2}$$

where m is the electron mass, $\Delta = U - \varepsilon$ is the height of the potential barrier and ε is the electron energy in the dot. For $a \gg \hbar/\sqrt{2m\Delta}$ Eq. (A2) yields

$$D \approx \frac{16\varepsilon\Delta}{U^2}\exp\left(-\frac{2\sqrt{2m\Delta}}{\hbar}a\right). \tag{A3}$$

One can think about the electron bouncing back and forth within the potential well of the dot with an average velocity $v = \sqrt{2\varepsilon/m}$. The average time between its collisions with the "wall" of the potential is approximately $2l/v$, so the frequency of collisions is $v/2l$, where l is the size of the quantum dot (well). The probability that the electron tunnels during any particular collision is D, so the probability of tunneling at any given time is $vD/2l$. Thus the tunneling time of electron from one dot to another is about

$$\tau = \frac{2l}{vD} \sim \tau_{\text{coll}} \cdot \frac{U^2}{16\varepsilon\Delta}\exp\left(\frac{2\sqrt{2m\Delta}}{\hbar}a\right), \tag{A4}$$

where

$$\tau_{\text{coll}} = 2l\sqrt{\frac{m}{2\varepsilon}} \tag{A5}$$

is the collision time of electron with the walls of the dot. For $l = 8$ nm and $\varepsilon = 0.1$ eV we obtain $\tau_{\text{coll}} = 0.85 \times 10^{-13}$ s.

The tunneling time τ should be much smaller than time of electron-hole recombination in the quantum dot

$$\tau \ll \tau_{\text{rec}} \tag{A6}$$

which yields limitation

$$a \lesssim \frac{\hbar}{2\sqrt{2m\Delta}}\ln\left(\frac{\tau_{\text{rec}}}{\tau_{\text{coll}}}\frac{16\varepsilon\Delta}{U^2}\right). \tag{A7}$$

For $\varepsilon = 0.1$ eV, $\Delta = 0.9$ eV, $U = 1$ eV, $\tau_{\text{coll}} = 10^{-13}$ s and $\tau_{\text{rec}} = 10^{-8}$ s Eq. (A7) yields

$$a \lesssim 1 \text{ nm}. \tag{A8}$$

So, in order to have efficient tunneling the quantum wells (dots) must be very close to each other.

Appendix B High precision quantum dot processing

Semiconductor quantum dot nanocrystals are prepared by a variety of techniques and are available commercially. For example, solutions of CdS quantum dots covering the spectrum from 360 nm to 460 nm and CdSe dots going from 460 nm to 650 nm can be purchased. For some quantum solar cells it may suffice to use these semiconductor quantum dots "as-is". However, in the case we envision, it will be useful to have a finer control on the dot sizes.

We here present a simple and potentially inexpensive means of precision sorting of an ensemble of quantum dots.

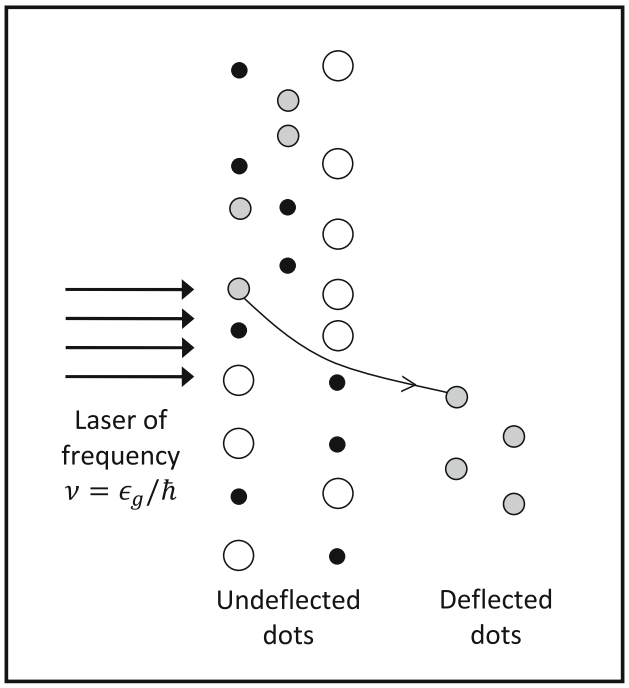

Fig. 10 Laser deflection of falling quantum dots according to optical resonant energy $\hbar\nu = \epsilon_g$

In Fig. 10 we show an inhomogeneous powder of quantum dots having a wide distribution of sizes. The dots are dropped in vacuum or other medium (e.g. inert gas) and subjected to a dot band gap sequence of (e.g. semiconductor diode) laser beams tuned to a particular quantum resonant frequency.

Now when a dot absorbs or emits a photon of frequency ν from a light beam, a transfer of recoil momentum $\Delta p = \hbar k = \hbar\nu/c$ takes place between the dot and the field. If absorption is followed by spontaneous emission, there is a net momentum transfer to the dot as the spontaneous emission goes in 4π steradians and gives no average contribution. Hence, as shown in Appendix C, the force on a dot due to this absorption and emission of laser photons is given by

$$F = \frac{1}{2}\Gamma\hbar k\ , \tag{B1}$$

where Γ is the radiative decay rate and $\hbar k$ is the momentum of a photon of wave vector k.

Then, as is shown in the following example, a substantial deflect of ≈ 1 cm can be achieved with inexpensive diode lasers.

To estimate the deflection we note that the vertical position of a quantum dot falling in vacuum in the earth's gravitational field is given by $\frac{1}{2}gt^2$ and the deflection is then $x = \frac{1}{2}\frac{F}{m}t^2 = \frac{F}{m}\frac{y}{g}$. Hence, using Eq. (B1) for F, we obtain

$$x = \frac{\Gamma\hbar k}{2mg}y. \tag{B2}$$

The buffer gas molecules would exert a viscous force on the quantum dot proportional to the quantum dot velocity. This changes $x(t)$ and $y(t)$, but not the ratio $x(t)/y(t)$. As a consequence, presence of the viscous force does not change Eq. (B2).

We may then calculate the deflection from Eq. (B2) by taking the reasonable case of a 10 nm dot of CdSe having mass $m \simeq 10^{-19}$ kg, $g \simeq 10$ m/s^2, $\Gamma \sim 10^8$ s^{-1} and a 500 nm photon having momentum $\hbar k \simeq \frac{1}{2}10^{-27}$ kg $\cdot$ m/s for which the ratio of radiation to gravitational force is of order 10^{-2}. Hence we find a substantial 1 cm deflection when falling 1 m due to its interaction with an array of 100 milliwatt lasers each focused to 1 mm^2 for which the Rabi frequency $\Omega_R > \Gamma$. We note that this is well within the state of the art using inexpensive semiconductor diode lasers.

One should mention that non-destructive dispersion of quantum dots into a buffer gas has been experimentally demonstrated by Kumakura et al. [29], while size-separation of quantum dots by laser ablation has been demonstrated in liquid helium [30].

Appendix C Radiative pressure on a quantum dot

Upon absorbing a laser photon a dot experiences a momentum recoil of $\delta p = \hbar k$ upon each event and the force on the dot F is given by

$$F = r\hbar k, \tag{C1}$$

in which r is the rate of radiation decay given by

$$r = \Gamma\rho_{ee}, \tag{C2}$$

where Γ is the spontaneous emission rate from the excited state $|e\rangle$ to the ground state $|g\rangle$.

The interaction with a radiation field of frequency ν is described by the following set of equations for the density matrix of an effective two level atom describing the quantum dot exciton

$$\dot{\rho}_{eg} = -\left(i\Delta + \frac{\Gamma}{2}\right)\rho_{eg} + i\Omega_R\rho_{ee} - \frac{i}{2}\Omega_R, \tag{C3}$$

$$\dot{\rho}_{ee} = -\Gamma\rho_{ee} + \frac{i\Omega_R}{2}(\rho_{eg} - \rho_{ge}), \tag{C4}$$

$$\dot{\rho}_{ge} = \left(i\Delta - \frac{\Gamma}{2}\right)\rho_{ge} - i\Omega_R\rho_{ee} + \frac{i}{2}\Omega_R, \tag{C5}$$

where the detuning $\Delta = \omega - \nu$ and ω is the transition frequency. Here Ω_R is the Rabi frequency associated with the intensity of the light beam and the matrix element coupling states e and g. The steady-state solution of Eqs. (C3)-(C5) in the saturated limit $\Omega_R >> \Gamma$ is

$$\rho_{ee} = \frac{\Omega_R^2}{4\Delta^2 + \Gamma^2 + 2\Omega_R^2} \to \frac{1}{2} \tag{C6}$$

and from Eqs. (C1), (C2) and (C6) the absorptive force is found to be

$$F = \frac{1}{2}\hbar k\Gamma, \tag{C7}$$

which is in the same direction as the deflecting laser.

Appendix D Light absorption by quantum wells

Absorption and emission of light by quantum wells have been studied in details in connection with quantum well lasers. In particular, formulas obtained for the laser gain g (in cm^{-1}) can be used to estimate light absorption since absorption length $l_{\rm abs}$ is related to gain as $l_{\rm abs} = -1/g$. When gain is negative the incident light is being absorbed by the medium.

Here we estimate $l_{\rm abs}$ using Eq. (35) on page 36 of Ref. [31] which gives a general answer for gain valid for bulk semiconductors and quantum wells. In terms of the absorption length this equation reads

$$\frac{1}{l_{\rm abs}} = \frac{1}{\hbar\omega}\frac{\pi\hbar e^2}{\varepsilon_0 c m_e^2}\frac{\bar{n}_g}{\bar{n}^2}|M_T|^2\rho_{\rm red}(f_v - f_c), \tag{D1}$$

where e is the electron charge, m_e is the mass of bare electron, ε_0 is the permittivity of free space, c is the speed of light in vacuum, $\bar{n}$ is the index of refraction in the crystal, $\bar{n}_g$ is the group index of refraction

$$\bar{n}_g = \bar{n} + \omega\frac{d\bar{n}}{d\omega}, \tag{D2}$$

M_T is the transition matrix element, $\rho_{\rm red}$ is the reduced density of states at the energy $E = \hbar\omega - E_g$:

$$\frac{1}{\rho_{\rm red}} = \frac{1}{\rho_c} + \frac{1}{\rho_v}, \tag{D3}$$

f_c and f_v are Fermi-Dirac distribution factors for electrons in the conduction and valence bands

$$f_c = \frac{1}{1 + \exp\left(\frac{E_e - E_f}{k_B T}\right)}, \tag{D4}$$

$$f_v = \frac{1}{1 + \exp\left(\frac{E_h - E_f}{k_B T}\right)}. \tag{D5}$$

For parabolic conduction and valence bands the electron (hole) energy reads

$$E_e = E_c + \frac{\hbar^2 k_e^2}{2m_c}, \tag{D6}$$

$$E_h = E_v - \frac{\hbar^2 k_h^2}{2m_v}, \tag{D7}$$

where E_c and E_v are the band edge energies, m_c and m_v are the effective masses in the two bands and k_e, k_h are the magnitudes of the wavevectors of a given electron or hole.

For parabolic conduction and valence bands the reduced density of states $\rho_{\rm red}$ for a bulk 3D material is [31]

$$\rho_{\rm red} = \left(\frac{2m_{\rm red}}{\hbar^2}\right)^{3/2}\frac{\sqrt{E}}{4\pi^2}, \tag{D8}$$

where $m_{\rm red}$ is the reduced mass

$$\frac{1}{m_{\rm red}} = \frac{1}{m_c} + \frac{1}{m_v}, \tag{D9}$$

while for a quantum well (2D)

$$\rho_{\rm red} = \frac{m_{\rm red}}{2\pi\hbar^2}\frac{1}{L_{\rm QW}}, \tag{D10}$$

where $L_{\rm QW}$ is the quantum well thickness.

To estimate the absorption length one can take $f_v \approx 1$, $f_c \approx 0$ and $\bar{n}_g \approx \bar{n}$. Then Eq. (D1) reduces to

$$\frac{1}{l_{\rm abs}} = \frac{\alpha}{\bar{n}} \frac{|M_T|^2}{\hbar\omega m_e} \frac{4\pi^2\hbar^2\rho_{\rm red}}{m_e}, \tag{D11}$$

where α is the fine-structure constant

$$\alpha = \frac{e^2}{4\pi\varepsilon_0\hbar c} \approx \frac{1}{137}.$$

Substituting $\rho_{\rm red}$ for quantum well from Eq. (D10) we obtain

$$\frac{1}{l_{\rm abs}} = \frac{2\pi\alpha}{\bar{n}} \frac{|M_T|^2}{\hbar\omega m_e} \frac{m_{\rm red}}{m_e} \frac{1}{L_{\rm QW}}. \tag{D12}$$

So that the number of wells necessary to absorb incident light is independent of well thickness and given by

$$\frac{l_{\rm abs}}{L_{\rm QW}} = \frac{\bar{n}}{2\pi\alpha} \frac{m_e}{m_{\rm red}} \frac{\hbar\omega m_e}{|M_T|^2}. \tag{D13}$$

Let us consider quantum wells made of GaAs. We approximate $|M_T|^2$ by its bulk value (see Table 2 on page 49 of Ref. [31])

$$\frac{2|M_T|^2}{m_e} \approx 29 \text{ eV}, \tag{D14}$$

and take $m_c = 0.067m_e$, $m_v = 0.082m_e$ (that is $m_{\rm red} = 0.037m_e$). Then for $\hbar\omega = 1.6$ eV photons ($\bar{n} = 3.7$) we obtain that the necessary number of GaAs wells is

$$\frac{l_{\rm abs}}{L_{\rm QW}} = 240 \tag{D15}$$

which for 5 nm thick wells gives the absorption length of 1.2μm. Thus, the absorption length is of the order of the size of the depletion region.

For InP

$$\frac{2|M_T|^2}{m_e} \approx 20 \text{ eV}, \tag{D16}$$

$m_c = 0.077m_e$, $m_v = 0.64m_e$ ($m_{\rm red} = 0.069m_e$). Then for $\hbar\omega = 1.6$ eV photons ($\bar{n} = 3.7$) the necessary number of InP wells is

$$\frac{l_{\rm abs}}{L_{\rm QW}} = 187 \tag{D17}$$

which for 5 nm thick wells gives the absorption length of 0.9μm.

Absorption of photons by a bulk semiconductor is different due to different value of the density of states. However, difference is not substantial. Indeed, Eqs. (D8) and (D10) give that the ratio of the density of states for a bulk material and a quantum well is given by

$$\frac{\rho_{\rm bulk}}{\rho_{\rm QW}} = \sqrt{\frac{\hbar\omega - E_g}{E_{\rm QW}}}, \tag{D18}$$

where

$$E_{\rm QW} = \frac{\pi^2\hbar^2}{2m_{\rm red}L_{\rm QW}^2}. \tag{D19}$$

For 5 nm thick well with $m_{\rm red} = 0.069m_e$ Eq. (D19) yields $E_{\rm QW} = 0.2$ eV. Therefore, e.g., for $\hbar\omega - E_g = 0.5$ eV Eq. (D18) gives

$$\frac{\rho_{\rm bulk}}{\rho_{\rm QW}} = 1.6, \tag{D20}$$

that is absorption cross section of a bulk material is of the same order of magnitude as for quantum wells. The absorption length we estimated for GaAs (1.2 μm) and InP (0.9 μm) quantum wells of 5 nm thickness approximately agrees with those measured for the bulk materials near the absorption edge. One can say roughly that in order to absorb light by quantum wells the length of QW stack must match the absorption length of the bulk material.

References

1. M.O. Scully, Phys. Rev. Lett. **104**, 207701 (2010)
2. W. Shockley, H.J. Queisser, J. Appl. Phys. **32**, 510 (1961)
3. P. Würfel, *Physics of Solar Cells* (Wiley-VCH Verlag GmbH & Co. KGaA, Weinheim, 2009)
4. A.A. Svidzinsky, K.E. Dorfman, M.O. Scully, Phys. Rev. A **84**, 053818 (2011)
5. M.O. Scully, K.R. Chapin, K.E. Dorfman, M. Kim, A.A. Svidzinsky, PNAS **108**, 15097 (2011)
6. A.A. Svidzinsky, K.E. Dorfman, M.O. Scully, Coherent Opt. Phenom. **1**, 7 (2012)
7. M. Scully, S. Zubairy, G. Agarwal, H. Walther, Science **299**, 862 (2003)
8. C.H. Henry, J. Appl. Phys. **51**, 4494 (1980)
9. R.R. King et al., Appl. Phys. Lett. **90**, 183516 (2007)
10. R.R. King et al., Adv. Optoelectron. **2007**, 29523 (2007)
11. W. Guter et al., Appl. Phys. Lett. **94**, 223504 (2009)
12. P. Lumb et al., Adv. Energy Mater. **7**, 1700345 (2017)
13. J.F. Geisz et al., Nat. Energy **5**, 326 (2020)
14. K. Barnham, G. Duggan, J. Appl. Phys. **67**, 3490 (1990)
15. K.W.J. Barnham et al., Phys. E (Amsterdam) **14**, 27 (2002)
16. A. Nozik, Phys. E **14**, 115 (2002)
17. S.A. Blokhin et al., Semiconductors **43**, 514 (2009)
18. E.C. Cho et al., Nanotechnology **19**, 245201 (2008)
19. V. Aroutiounian, S. Petrosyan, A. Khachatryan, K. Touryan, J. Appl. Phys. **89**, 2268 (2001)
20. A. Alguno et al., Appl. Phys. Lett. **83**, 1258 (2003)
21. U. Aeberhard, R.H. Morf, Phys. Rev. B **77**, 125343 (2008)
22. S.R. Kurtz, J.M. Olson, A. Kibbler, in *High Efficiency GaAs Solar Cells Using GaInP2 Window Layers*. in Proceedings of the 21st IEEE Photovoltaic Specialists Conference
23. Sharp Corporation, Press Release, June (2013). https://global.sharp/corporate/news/130614.html
24. T. Takamoto, in *Status of Multijunction Solar Cells and Future Development*. Proceedings of the International Conference on Compound Semiconductor Manufacturing Technology (Tampa, Florida, 2009). https://csmantech.org/OldSite/Digests/2009/2009%20Papers/3.4.pdf
25. C.S. Jiang, H.R. Moutinho, D.J. Friedman, J.F. Geisz, M.M. Al-Jassim, J. Appl. Phys. **93**, 10035 (2003)

26. The present discussion follows M. Scully and S. Zubairy, *Quantum Optics* (Cambridge Press, 1997); See also the excellent treatment in Laser Cooling and Trappinged. by H. Metcalf, P. van der Straten (Springer, 1999)
27. M. Delong et al., Appl. Phys. Lett. **66**, 3185 (1995)
28. K. Leosson, D. Birkedal, I. Magnusdottir, W. Langbein, J.M. Hvam, Phys. E **17**, 1 (2003)
29. M. Kumakura et al., J. Phys. Conf. Ser. **1220**, 012039 (2019)
30. K. Inaba et al., Phys. Status Solidi B **243**, 3829 (2006)
31. S.W. Corzine, R.H. Yan, L.A. Coldren, in *Optical gain in III-V bulk and quantum well semiconductors*, ed. by P. Zory. Quantum well lasers (Academic Press, Inc., New York, 1993)